Current Opinion in Colloid & Interface Science 16 (2011) 135–148

Contents lists available at ScienceDirect

Current Opinion in Colloid & Interface Science

journal homepage: www.elsevier.com/locate/cocis

Nanoseparations: Strategies for size and/or shape-selective purification of nanoparticles

Bartlomiej Kowalczyk, István Lagzi, Bartosz A. Grzybowski *

Department of Chemistry and Department of Chemical and Biological Engineering, Northwestern University, 2145 Sheridan Road, Evanston, IL 60208, USA

ARTICLE INFO

Article history:
Received 1 September 2010
Received in revised form 4 January 2011
Accepted 5 January 2011
Available online 12 January 2011

Keywords:
Colloids
Fractionation
Nanoparticles
Purification
Separation

ABSTRACT

This paper reviews techniques currently available for size- and shape-selective purification of nanoscopic objects. The methods discussed range from variants of familiar chromatographic, centrifugation, or filtration techniques, to purification schemes deriving from nanoscale-specific phenomena, including shape-selective reactivity, or propensity to form organized superstructures.

1. Introduction

Nanoparticles can be synthesized in a wide variety of shapes [1*,2,3,4] and sizes, [5,6**,7] can have various material compositions [8–12] and surface modifications,[13–17**] and can exhibit size [18–21] or shape-dependent [22,23] properties. With numerous synthetic procedures now firmly in place, the focus of nanoscience is shifting toward the assembly of individual NPs into higher-order structures and nanomaterials with potential applications in sensors, [24**,25] drug carriers,[26,27**] supercapacitors, [28] diodes, [29,30] photonic [31] and photovoltaic [32,33] cells, or data storage media.[34,35] Some of the recent assembly schemes aim at using the nanoparticulate building blocks as "atoms" of more complex "nanomolecules".[36–39] While the analogies between nanoparticulate building blocks at the nanoscale and the atomic building blocks at the molecular scale appear appealing,[40,41] it must be remembered that NPs – unlike atoms – are never monodisperse and no two particles are ever identical. This inherent polydispersity complexifies self-assembly and affects the overall characteristics deriving from the size-dependent properties of individual NPs (e.g., surface plasmon resonance, SPR, [42,43] or magnetic susceptibility [44,45]).

Therefore, in order to synthesize nanostructured materials/devices with well-defined properties and functions, it is desirable to reduce the polydispersity of their nanoparticulate components. The ability to tailor low-polydispersity particles is important in, for example, catalysis where catalytic activity of the NPs[46,47] depends on the particle size and shape (the latter being related to the nature of crystal planes exposed), biology and medicine (e.g., cytotoxicity of AuNPs is size dependent),[18,48,49] or in nanodevices where only NPs of a given size contribute to the overall properties of the device. [50,51**] In several cases (e.g., using polymeric stabilizers, [52,53] reverse micelles, [54] or thermal decomposition methods [55]), low degree of polydispersity can be achieved during particle synthesis; in many others, however, the particles need to be purified post-synthesis. In addition, for non-spherical particles (e.g., nanorods, prisms, or cubes [56**,57*,58]) solution-based procedures yield target particles contaminated with differently shaped objects, including small spherical "seeds" and other competing particles. In this review, we highlight some recent developments in the purification of both spherical and non-spherical nanoparticles based on the phenomena ranging from magnetics, through electrophoresis, filtration and chromatographic methods, to chemical or biochemical purification.

This review is aimed at a broad audience of scientists who don't specialize in analytical chemistry but use nanoparticles in biology, materials chemistry, catalysis, self-assembly, or nanotechnology. It is our hope that the overview of various separation techniques along with a critical commentary might help choose a separation method that is best suited to a specific research project.

2. Methods of NPs fractionation

2.1. Separation of NPs by magnetic fields

Magnetic fields can separate NPs according to their magnetic susceptibilities and/or sizes. The magnetic force which acts on a particle is given by $F_M = \mu_0 \chi V_p H \nabla H$, where H is an external magnetic field, χ is the magnetic susceptibility, and V_p is particle's volume.

* Corresponding author.
E-mail address: grzybor@northwestern.edu (B.A. Grzybowski).

1359-0294/$ – see front matter © 2011 Published by Elsevier Ltd.
doi:10.1016/j.cocis.2011.01.004

It has been estimated [59] theoretically that the limiting size for separation of iron oxide NPs in the low magnetic field gradients (<100 T/m) is ~50 nm. For smaller NPs, thermal diffusion (thermophoresis) and Brownian motions overcome the magnetic forces acting on the particles and successful fractionation is not possible. However, these theoretical works extrapolated NP properties from those of the bulk materials, which is not warranted for nanoscale objects exhibiting transition to a single domain character (e.g., at room temperature, iron oxide nanoparticles smaller than 26 nm are superparamagnetic, while larger ones are ferromagnetic [60••]). Also, theoretical calculations usually ignore dipole–dipole interactions between particles' magnetic moments, which might be present even in the absence of external magnetic fields. These interactions can cause formation of large NP aggregates characterized by strong magnetic response (due to increased apparent V_p). In fact, such aggregates were observed experimentally by Moeser et al. [61] during high gradient magnetic separation (HGMS) of magnetic nanoparticles. Interestingly, formation of aggregates could also explain why it is possible to separate NPs smaller than predicted by theory [61,62].

The work by Yavuz et al. [63•] illustrates well the potential and usefulness of magnetic separations under experimentally feasible conditions (fields <1–2 T, field gradients <100 T/m). These authors demonstrated efficient separation of differently sized Fe_3O_4 NPs on a column packed with steel wool and subject to a tunable magnetic field. The influence of the field on the retention of separate batches of differently sized (4, 6, 9.1, 12, and 20 nm) nanocrystals was demonstrated by HGMS with higher fields required to retain smaller particles on the column (since $F_M \propto V_p$).

Another system, based on the so-called capillary magnetic field flow fractionation (MFFF) and described by Latham et al., [64] demonstrates that magnetic NPs can be separated not only according to size but also to material composition. This technique relies on the competition between (i) magnetic forces acting perpendicular to the capillary flow and of magnitude proportional to the particles' magnetic susceptibility; and (ii) hydrodynamic forces and particle diffusion. The balance between these effects separates the particles into distinct "bands" such that larger particles (which interact stronger with the field) are retained in the column more efficiently, and therefore have longer elution times comparing to smaller particles (Fig. 1a). The use of this method was illustrated in reference [64] where the mixture containing 6 nm maghemite (γ-Fe_2O_3) and 13 nm cobalt ferrite ($CoFe_2O_4$) NPs was, owing to strong dependence of NP retention times on particle composition (Fig. 1b), successfully separated into two monodisperse fractions. It must be stressed, however, that in this method careful tuning of experimental parameters (e.g., solvent flow rate) is crucial for a good quality fractionation.

In principle, magnetic NPs could also be separated by general methods applicable to nonmagnetic particles (e.g., centrifugation, chromatography, and electrophoresis). In an interesting study, Rheinländer et al. [65] compared the efficiency of magnetic (MFFF) and nonmagnetic (size-exclusion chromatography, SEC) fractionation methods applied to iron oxide nanoparticles. Two batches of polydisperse magnetic fluids with different average NP sizes (5–6 nm and 8 nm) were tested. Smaller particles were stabilized with dextran (polymeric carbohydrate) and larger ones with poly(ethylene glycol), both soluble in water. In the case of magnetic fractionation on a column filled with soft magnetic iron spheres (0.3 mm in diameter), size of NPs in collected fractions increased with increasing retention time and with decreasing magnetic field. In contrast, SEC gave fractions in which average NP size decreased with elution time. Both techniques however, gave very similar results, yielding NP fractions with almost identical magnetic properties. Although the methods appear equivalent in terms of efficiency, the authors point out few practical advantages of magnetic fractionation over chromatography. First, SEC often requires addition of a surfactant (see Section 2.2), which often destabilizes magnetic fluids. Second, there is a limited number of column materials for SEC separation of larger particles (which can be easily separated by low magnetic fields). Third, magnetic-field methods are generally faster than SEC.

2.2. Chromatography

In chromatographic separations, a mobile phase containing a mixture to be separated passes through a stationary phase. The separation is then based on the differences in the partition coefficients between mobile and stationary phases for all components of the mixture. While several examples of the use of HPLC for NP separation have been reported, [66,67] size exclusion chromatography, SEC, is probably the most popular chromatographic technique used to fractionate nanoparticles. SEC is based on the differences in the particles' hydrodynamic volumes and not on the interaction of these particles with the stationary phase. Small particles meander freely through the pores around the stationary phase and thus travel through the column slowly. In contrast, large particles which do not fit inside the pores of the stationary phase, can travel only through the accessible volume (~30% of total volume) and elute more rapidly.

SEC has been used in the separations of different types of nanoparticles, including gold, [68] silica, [69] and semiconductor ones. [70] For successful resolution of a mixture by SEC, proper eluent and stationary phase (specifically, proper pore size of the stationary phase) have to be chosen, and irreversible adsorption of NPs onto the stationary phase (clogging its pores) should be avoided. To remedy the latter problem, Wei and Liu[71,72] added sodium dodecylsulfate (SDS) anionic surfactant to the mobile phase. The idea here was that the negatively charged surfactant adsorbing onto the stationary phase would electrostatically repel the negatively charged (here, citrate-functionalized) NPs thus preventing their sorption on the column. Using a column loaded with 8 μm polymeric particles with pores ~100 nm the authors showed that the efficiency of separation of 5.3 nm and 38.3 nm, citrate-functionalized AuNPs increases with surfactant concentration.

The same authors have also shown that surfactant-assisted SEC is a feasible method for separating NPs based on their shapes. [73] The mixture they used comprised 85% of relatively monodisperse gold nanorods (~9.7 nm minor axis diameter, aspect ratio ~1:4.8) and 15% of spherical particles (~19.3 nm in diameter). Without any surfactant added, adsorption of the particles of both types onto the stationary phase was so strong that no signal was detected (curve [a] in Fig. 2). Upon the addition of SDS, [b], strong signal corresponding to NPs of both shapes was obtained but the resolution was very poor. Finally, efficient separation was achieved, [c], by using a mixture of surfactants, SDS and polyoxyethylene (23)dodecanol (Brij-35). A plausible explanation of the role of Brij-3 is that this nonionic surfactant partly replaces SDS from the surfaces of the NRs/NPs. As a result, surface charge of these particles decreases and their adsorption onto the stationary phase increases (since particle/matrix electrostatic repulsions are weakened [71]). Because such adsorption is shape-dependent, there is more differentiation between particles of different shapes translating into a higher-quality separation.

SEC is a rapidly developing technique, constantly adapting to new challenges. Recently, Al-Somali et al. [74,75] introduced the so-called "recycling SEC", which significantly improved the resolution of the technique and made it more suitable for nanoscience applications. Recycling SEC allows for increasing the effective column length by returning the output back into column for several more runs. The resolution increases with each run and exhibits a square root dependence on the number of runs. With this technique, it was possible to separate alkyl-thiol-stabilized gold nanoparticles differing in size by only 6 Å. Other types of NPs (e.g., CdSe) were also successfully separated with remarkable precision.

Another example of application of SEC as an efficient nanoseparation technique was provided by Novak et al. [76] who reported the purification of monomer AuNPs from nanoparticle dimers, trimers and tetramers in which the NPs were linked covalently by, respectively,

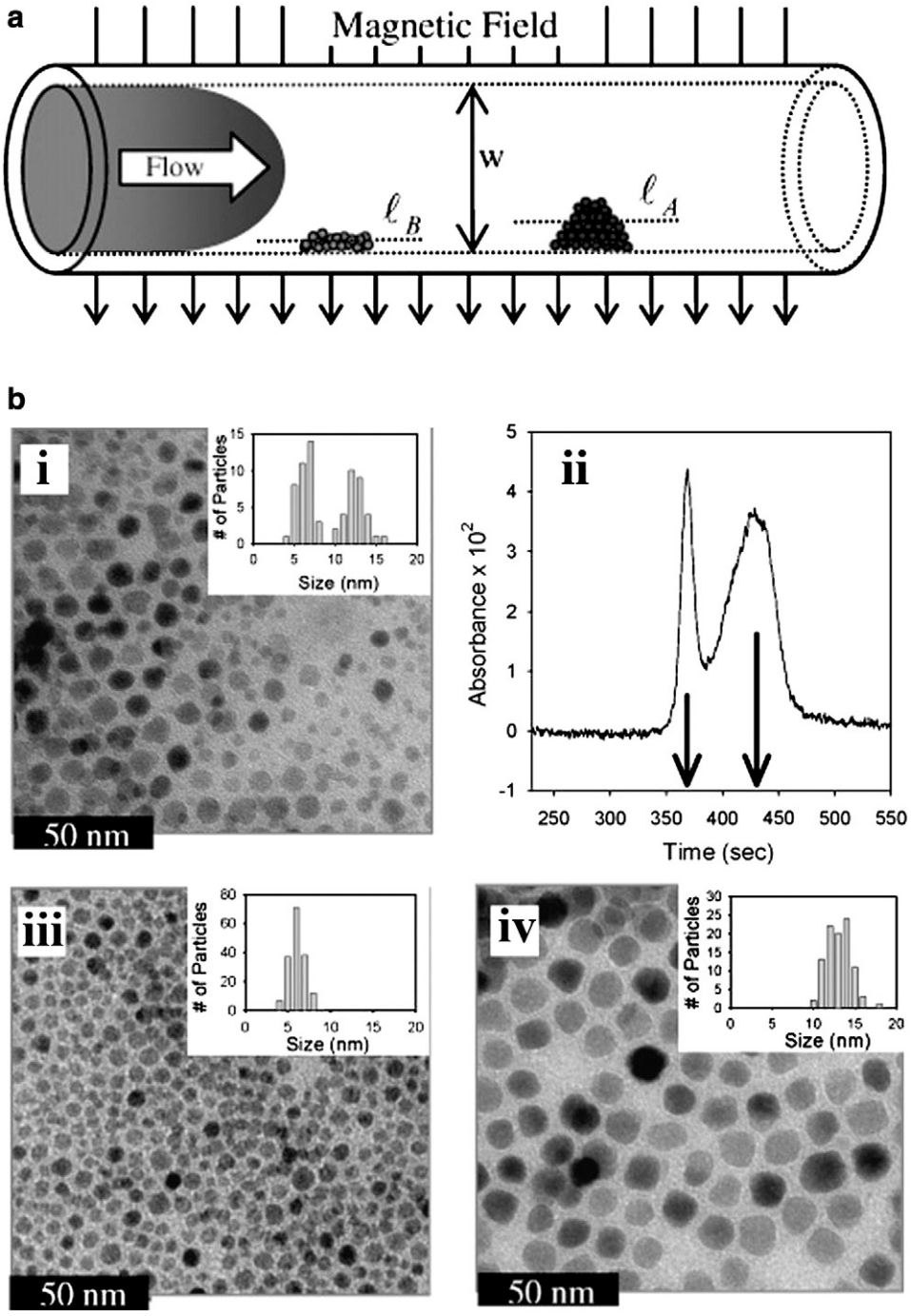

Fig. 1. (a) Scheme illustrating the principle of MFFF for magnetic particles in a capillary channel subject to an applied magnetic field. Particles that interact weakly with the magnetic field have a large average layer thickness (l_A) and elute at shorter times; strong interaction results in smaller layer thickness (l_B) and longer retention times. (b) (i) TEM image of a mixture of 6 nm Fe_2O_3 and 13 nm $CoFe_2O_4$ nanoparticles. (ii) MFFF of a 1.3 μL aliquot of a hexane solution of this mixture with a flow rate ramped from 5 to 50 μL/min. Arrows indicate times when the fractions shown in the TEM images in (iii) and (iv) were collected. All TEM scale bars are 50 nm; image insets contain histograms of the particle size distributions. Figure was taken from the Reference [64].

phenylethynyl di-, tri- and tetrathiols (Fig. 3). The authors compared the results of their SEC separation with the outcome of centrifugation. Obtaining similar results for both techniques, they concluded that one advantage of SEC is the possibility of direct/immediate post-column optical and electrochemical analysis of collected fractions using an automated setup (e.g., with UV–Vis coupled directly to chromatography), while NP aggregation and binding to the stationary phase is a disadvantage of the method. On the other hand, centrifugation is simpler and less expensive than SEC. Centrifugation (combined with density gradients) will be described in more detail in the next Section.

2.3. Density gradient centrifugation

Centrifugation is one of the most important separation techniques used widely in colloid science and in cellular and molecular biology. [77] While objects denser than a liquid settle spontaneously due to gravity, this process can take very long; for very small particles (e.g., nanoparticles, nanotubes) where gravitational energy is commensurate with thermal energy, the particles will not settle at all. However, centrifugal forces can help particles to move radially away from the axis of rotation and can separate these particles by size and shape. In a

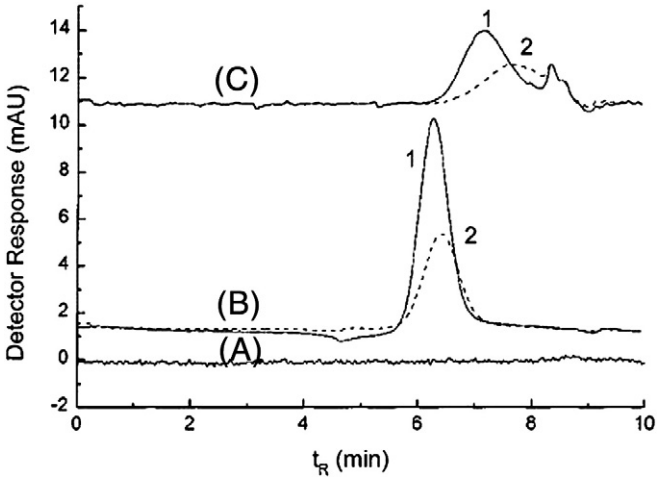

Fig. 2. SEC separation of nanorods (2) and nanospheres (1) under different composition of surfactants added to the eluent: (A) no surfactants added; (B) 40 mM SDS; (C) 40 mM SDS and 30 mM Brij-35. Figure was taken from the Reference [73].

centrifugal field, three main forces act on a particle: centrifugal force ($F_c = \rho_p V\omega^2 r$), buoyant force ($F_b = -\rho_f V\omega^2 r$), and frictional force ($F_f = -fv$). Here, ρ_p, ρ_f are the density of the particles and the fluid, respectively, V is particle's volume, ω is angular velocity, r denotes the distance of the particle from the axis of rotation, f is the frictional coefficient (in general, depending on particle shape and size), and v is particle's velocity. The particle will be accelerated in a centrifugal field until the forces balance, $F_c + F_b = F_f$, and will afterwards sediment with a constant velocity $v = \frac{V(\rho_p - \rho_f)\omega^2 r}{f}$. The fact that particles of different sizes and/or shapes move with different velocities in the medium provides a basis for particle separation into distinct bands, though the quality of separation is poor if the particles are similar — to remedy this, more powerful techniques are needed.

One such technique is the density gradient centrifugation, in which particles are centrifuged in a liquid column supporting a density gradient (such that the buoyant force varies within the tube). Density gradient can be created by careful layering of the different-concentration liquids on top of one another — as a result, density increases from the top to the bottom of the tube. There are two variants of this technique: (i) isopycnic centrifugation and (ii) rate zonal centrifugation.

In the isopycnic technique, the densities of the objects to be separated must be between the lowest and the highest densities of the column's gradient. The sample is usually applied as a thin layer at the top of the gradient. Each of the particles will sediment only to the position in the centrifuge tube at which its density is equal to that of the gradient; there, it will remain. The isopycnic technique, therefore, separates particles into zones solely on the basis of their buoyant density differences. The run time must be sufficient for the particles to separate to their isopycnic points, but excessive centrifugation times have no further effect on the position of the bands.

In the rate zonal centrifugation, RZC, the sample has the density greater than that of the highest density portion of the gradient. The sample is applied as a thin layer at the top of the tube and, during centrifugation, the particles begin sedimenting through the gradient into separate zones according to particle size, shape, and density. In contrast to the isopycnic technique, however, the separation must be terminated before the separated particles reach the bottom of the tube.

In both RZC and isopycnic methods, particles from different bands can be easily removed by a needle or a pipette syringe. The fractions can be purified by several centrifugation–redispersion cycles using an appropriate solvent.

Isopycnic centrifugation has been applied successfully for diameter-dependent separation of single-walled carbon nanotubes (SWNT). [78•,79] On the other hand, this method is not applicable to metallic/inorganic nanoparticles which are usually denser than the highest densities achievable in aqueous media gradients (<~1.7 g cm^{-3}). [80] Given this limitation, "heavy" nanoobjects should be separated by RZC (which is, of course, also applicable to "lighter" nanoparticles, as in the reported diameter separation of SWNTs using structure-discriminating surfactants). [81] An appealing feature of RZC methods is that the times of separation can be as short as 15 min compared to hours in typical isopycnic methods.

For example, Sun et al. [82] used RZC to separate FeCo@C (FeCo nanoparticles coated in graphitic shells) and gold nanoparticles (Au NPs). Controlling the step gradient densities and centrifugation times, polydisperse FeCo@C NPs of a larger (on average, 7 nm) and smaller (on average, 4 nm) size ranges were separated. In all experiments, the step gradients were created in a centrifuge tube by layering different concentration of iodixanol solutions, and the nanoparticle solutions were layered on top of the density gradient. FeCo@C NPs with average diameters of about 4 nm were successfully separated using a 10% + 20% + 30% + 40% gradient. After centrifugation, several distinct bands formed in the centrifuge tube

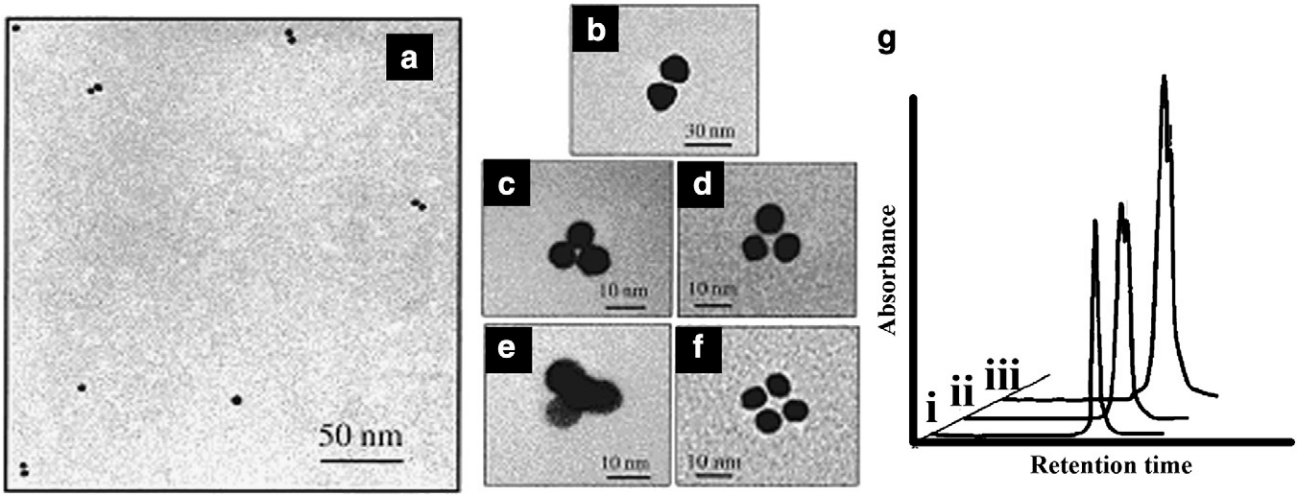

Fig. 3. (a–f) TEM images of dimer, trimer and tetramer "nanomolecules" held by covalent links between 10 nm AuNPs. (g) Chromatographs of 10 nm AuNPs (i), their dimers (ii), and trimers (iii). Two distinct but poorly separated peaks are visible in (ii) and (iii), corresponding to the separation of single nanoparticles from dimers and trimers, respectively. Figure was taken from the Reference [76].

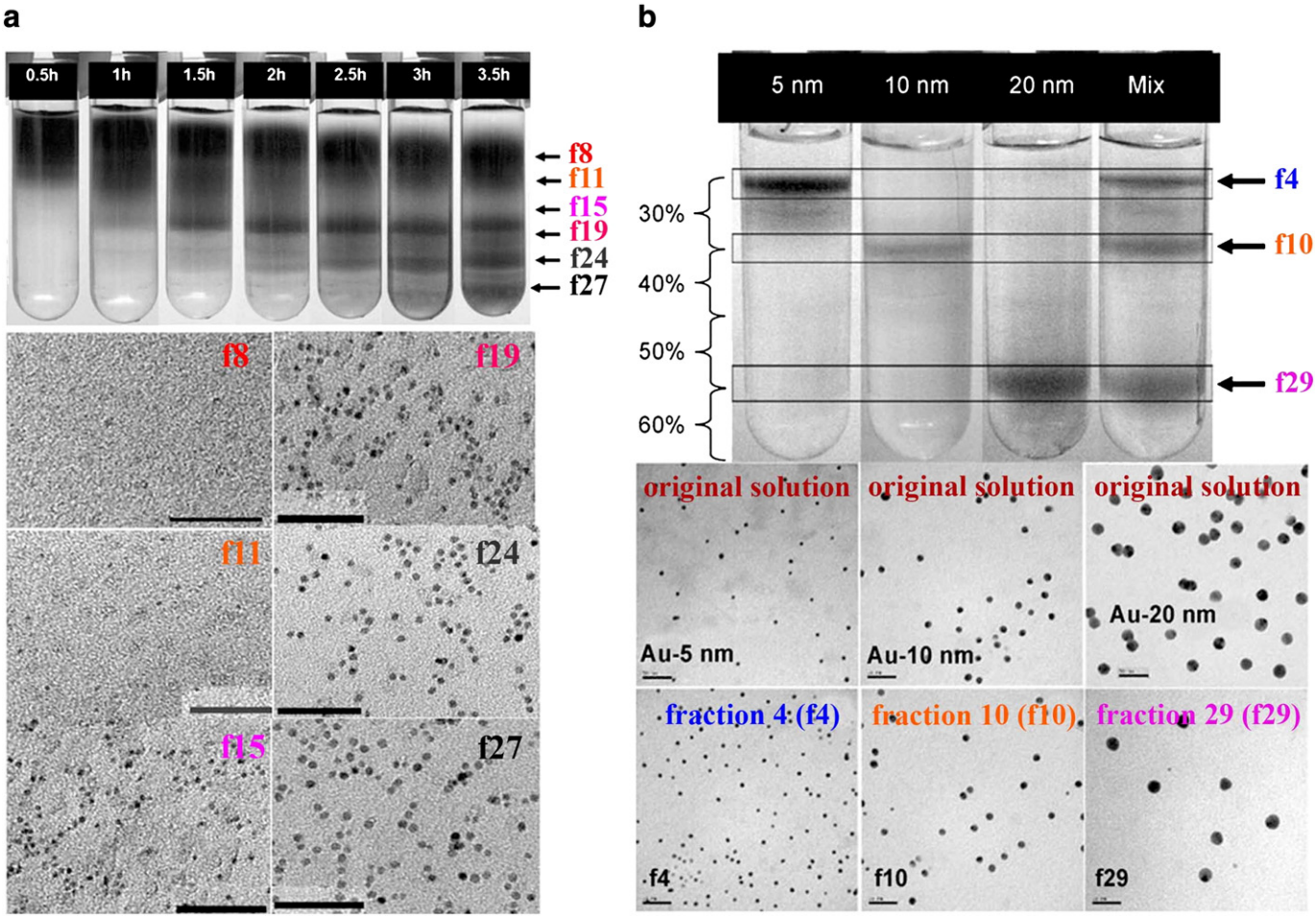

Fig. 4. Optical and TEM images illustrating the separation of (a) 4 nm FeCo@C nanoparticles and (b) Au NPs using the rate zonal centrifugation technique. Scale bars correspond to 50 nm. Figure was taken from the Reference [82].

corresponding to the separation of NPs of different sizes (Fig. 4a). Sampling these fractions (bands) along the centrifuge tube provided nanoparticles of sizes increasing from 1.5 nm to 5.5 nm NPs. For larger FeCo@C NPs (on average 7 nm) a gradient of higher density steps (20%+30%+40%+60%) was used. Similar to the previous experiment, a banded structure appeared in the centrifuge tube. Each band (fraction) along the tube contained different sizes of NPs, from 2 to 9 nm. This method was also successfully applied for the separation of Au NPs of different sizes (5 nm, 10 nm, and 20 nm) using a 30%+40%+50%+60% gradient. Here the centrifugation time was significantly shortened (15 min) compared to 2–3 h in the FeCo@C experiments. Due to the AuNPs' SPR in the visible range, the bands had characteristic red to violet hues (Fig. 4b).

Centrifugation was also used to separate dimers and trimers of gold nanoparticles. [83] Specifically, Chen et al. synthesized AuNP clusters ($AuNP_n$) covered with polystyrene-block-poly(acrylic acid) ($AuNP_n$@PSPAA) and separated them using a step density gradient centrifugation. A concentrated solution of $AuNP_n$@PSPAA was carefully layered on top of a 11%+62% CsCl gradient, and was then centrifuged for 20 min. Two distinct bands (red and purple in color) were obtained (Fig. 5). The red band contained mostly monomers. The purple band (b2 in Fig. 5) was extracted and purified twice to remove excess CsCl, it was found to contain ~95% dimers. To enrich the trimers, the components remaining after extraction of monomers and dimers were combined and excess CsCl was removed. This sample was then used for a further separation on a 11%+62% CsCl gradient. The three resulting bands had different colors and contained different proportions of trimers (Fig. 5, c3). The lowest band (c3) contained mostly trimers (~81%). At longer centrifugation times, bands shifted downward, while the gap between them increased.

Lastly, centrifugation has been used to separate non-spherical particles. As an example, we consider gold nanorods, AuNR, whose solution-based synthesis invariably gives a large proportion of spherical or polyhedral (mostly cubical) AuNP byproducts. Depending on the method, the fraction of by-products can be from 10% to almost 90%. Sharma et al. [84] have recently described separation of AuNRs and AuNPs by centrifugation at 5600 *g* for 30 min. The results showed that spheres and cubes sediment at the bottom, segregating from rods that form a high-purity deposit on the side wall (Fig. 6a and b). The UV–Vis–NIR spectrum of the solution of nanoobjects retrieved from the side walls shows an intense and red-shifted (compared to the original mixture) SPR peak at 1080 nm characteristic of AuNRs. In contrast, the spectrum of the particles retrieved from the bottom of the test-tube is blue shifted from the original solution suggesting more spherical NPs. These conjectures are verified by direct TEM imaging of the two fractions (Fig. 6d and e).

The separation can be attributed to the differences in the equilibrium sedimentation velocities of rods and spheres, $v_0^{rod}/v_0^s = 6(D/2a)^2[2\ln(L/D) - (v_\perp + v_\parallel)]$, where a is the radius of the sphere, L and D are the diameter and the length of the rod, respectively, and $v_\perp, v_\parallel$ are the correction factors for the rod (perpendicular and parallel to the rod's long axis). As seen, the v_0^{rod}/v_0^s ratio depends predominantly on the ratio of the squares of the NP/NR diameters. In experiments described by Sharma and co-workers, the average diameter of the spherical particles was 16 nm, whereas the average diameter of NRs was 8 nm. It thus follows that spherical particles

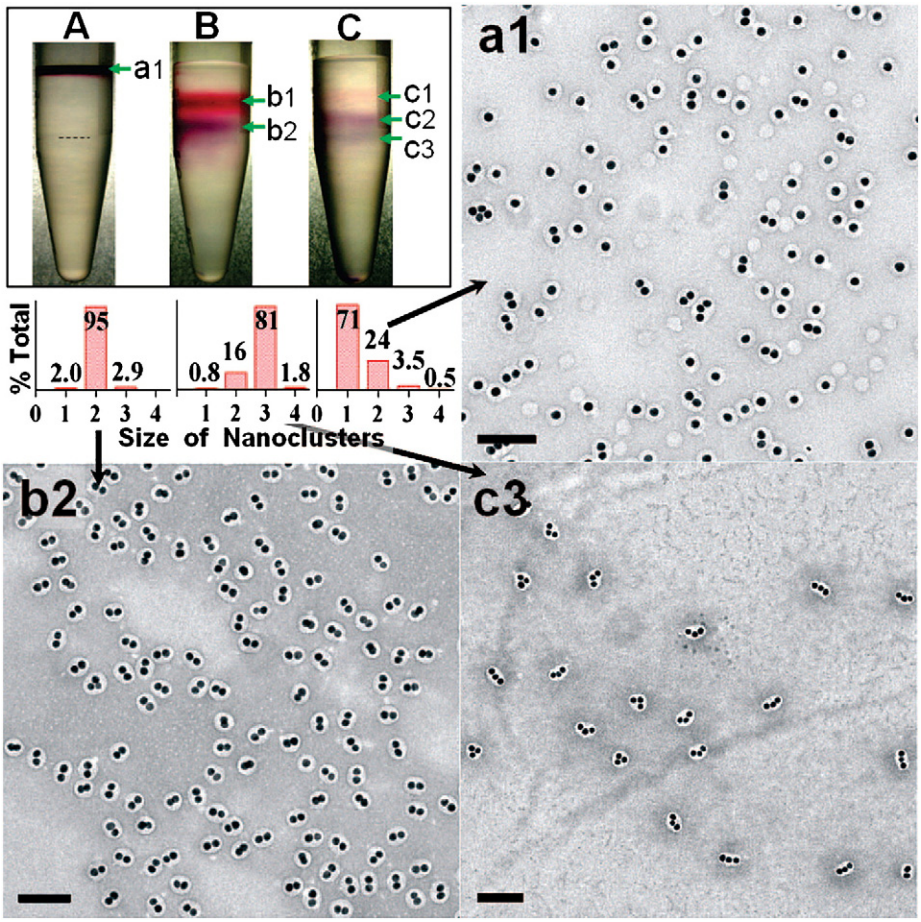

Fig. 5. Separation of $AuNP_n$@PSPAA particles (monomers, dimers, and trimers) in a 11% + 62% CsCl density gradient. TEM images of the respective fractions indicated in A–C. Scale bars correspond to 100 nm. Figure was taken from the Reference [83].

sediment faster than rods, and the spheres are enriched at the bottom of the test-tube while the rods deposit on the side-walls.

2.4. Electrophoresis

Electrophoretic techniques can separate charged objects in a uniform electric field. These methods are used widely in biological and biochemical research, protein chemistry, and pharmacology.[85] Charged molecules or particles migrate in an electric field toward the opposite-polarity electrode. For low Reynolds numbers characterizing the system and for moderate electric field strength, E, the steady-state velocity of a particle is linearly proportional to the applied field: $v = \mu_e E$. In this expression, μ_e is the electrophoretic mobility proportional to the particle's charge and inversely proportional to frictional forces acting on the particle (these forces depend on the particle's shape and size). Overall, particles having different charges, sizes, or shapes have different migration velocities and ultimately separate into distinct bands.

The most popular electrophoretic modalities are gel electrophoresis (GE), free flow electrophoresis (FFE), and isoelectric focusing (IEF) electrophoresis. In the familiar GE, [44] the particles migrate through a gel matrix (e.g., agarose or PAA — polyacrylamide). In FFE, a thin film of an electrolyte solution flows laminarly between two parallel plates. [86] An electric field is applied perpendicular to the flow resulting in a differential deflection of charged particles injected in the channel. This technique combines the high resolving power of electrophoresis with continuous-flow separation and yields large quantities of separated species within a short period of time. Finally, IEF electrophoresis is used extensively in biology to separate isoforms of proteins according to their isoelectric point (pI). In a typical IEF arrangement, charged biomolecules migrate in a pH gradient immobilized in a PAA gel. The pH range is generated by immobilines, weak acids or bases of defined pK_a values, covalently linked to PAA gel backbone. Upon application of an electric field, objects reach their points of zero charge (i.e., $pH_{gel} = pI$).

These techniques have been recently applied in nanoscience. For example, Hanauer et al. [87] used GE to separate polymer-coated spherical, rod-shaped, and triangular gold and silver nanoparticles. They synthesized the gold and silver NP samples using the seeded growth technique and coated these NPs with thiolated polyethylene glycols terminated in carboxylic groups (SH-PEG-COOH). Experiments were run in a 0.2% agarose gel, in a pH = 9 buffer for 30 min at 150 V (15 cm electrode spacing). Four types of samples were loaded onto one gel: a silver sample (which contained 13% rods, 34% spheres, 44% triangles, and 9% other shapes), gold rods, gold spheres, and the mixture of the gold rods and gold spheres. After GE, the gel shows different colors in the silver lane and clear separation of gold spheres (red) mixed with gold rods (green) (Fig. 7). The colors are due to the size- and shape-dependent optical properties of gold and silver particles and indicate separation according to nanoparticle morphology.

The inhomogeneous silver sample was analyzed further by Transmission Electron Microscopy, TEM. Fig. 8 shows representative TEM images obtained from the indicated positions within the gel. For each of these four locations, 100 particles were chosen and classified according to their shapes (rods, spheres, or triangles). Rods were located predominantly in the fraction containing the lowest-mobility

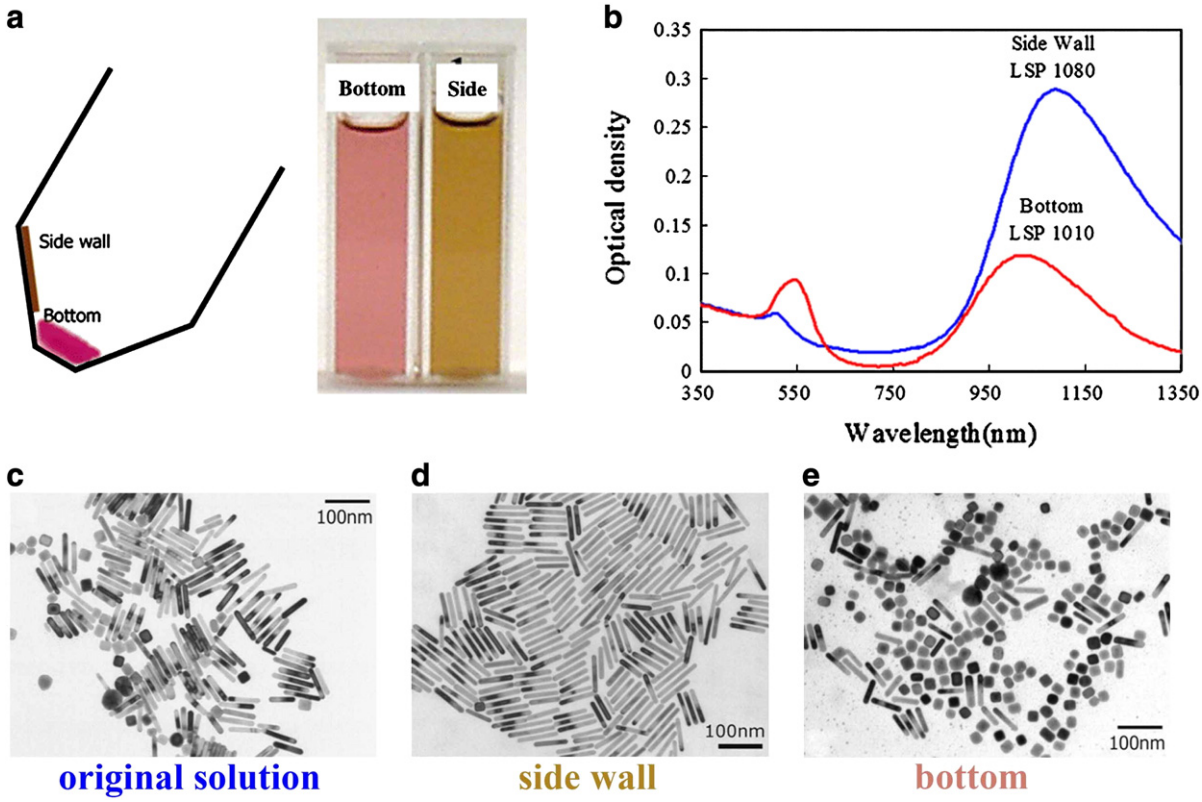

Fig. 6. (a) Separation of nanoparticles and the color of the NP solution taken from two different locations (bottom and side wall). (b) UV–Vis–NIR spectra of the solutions (c) TEM image of the original solution (mixture of nanorods and spherical and cubic nanoparticles). (d) TEM of nanorods deposited on the side wall of the tube after centrifugation. (e) TEM of a mixture of spheres, cubes, and larger-diameter nanorods sedimented at the bottom of the tube. Figure was taken from the Reference [84].

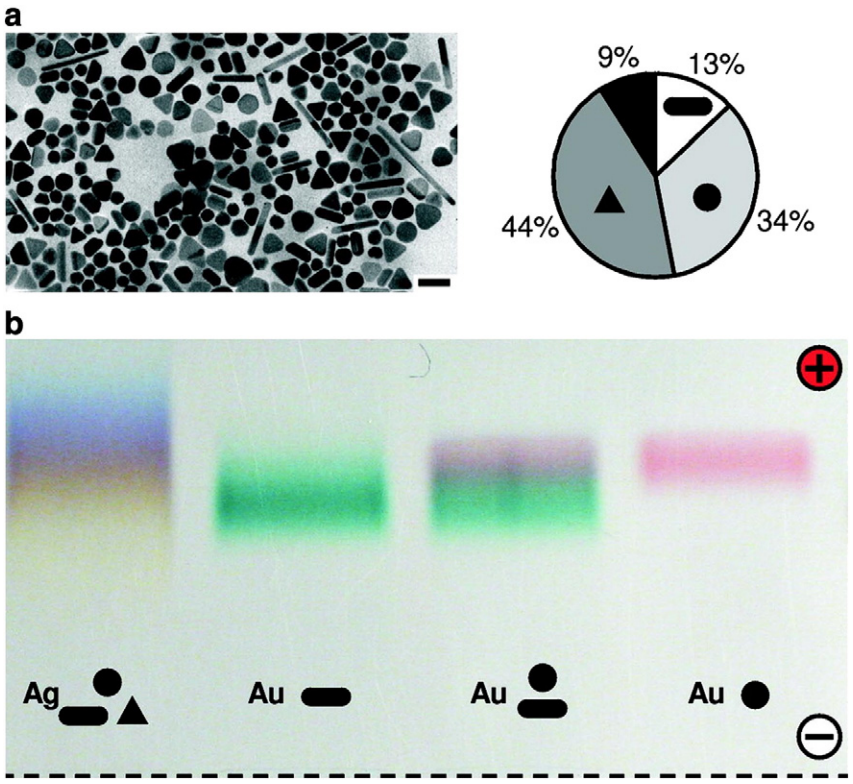

Fig. 7. TEM picture of a silver NP sample (left, scale bar 100 nm) and the proportion of spheres, triangles, and rods (right). (b) Optical micrographs of agarose gels supporting GE of nanoparticle mixtures. The dashed line at the bottom indicates the position of the gel wells. The four lanes contain, from left to right, silver nanoparticles, gold NRs (40×20 nm), gold rods and spheres mixed just before electrophoresis, and spherical gold NPs (15 nm) as indicated symbolically. Figure was taken from the Reference [87].

particles; in this band, the content of rods was ~60% vs. 13% in the original mixture. In contrast, spheres showed a slight tendency to accumulate in the faster-moving fractions. The triangles were clearly enriched in the fastest-moving fraction (50% vs 20% in the slowest fraction). For the NRs, aspect-ratio was inversely related to the migration speed: the average aspect ratio was 8.3 ± 0.8 in the slowest-moving fraction, compared to 3.1 ± 0.7 in the fastest one. For the spherical particles, a clear trend of increasing mobility with increasing size was observed: the average diameter of the spheres increased from 41 ± 2 nm to 65 ± 2 nm from the slowest- to the fastest-moving fraction. The mobility of the triangles showed no clear trend.

Separation of semiconductor NPs by FFE was described by Ho et al. [88] In this work, CdTe NPs were stabilized with negatively charged thioglycolic acid, TGA. Carrier buffer (pH 11) was pumped into buffer inlets to create laminar flow in the channel and the CdTe solution was infused through the sample inlet (Fig. 9a). Effect of temperature on the quality of separation was investigated systematically from 2 °C to 50 °C. At lower temperatures, diffusion and mixing were minimized and the quality of separation was better; in addition, above 50 °C and in the presence of electric field, the buffer boiled. Consequently, the channel temperature was maintained at 2 °C. A high electric field (1 kV) was applied perpendicular to the flow direction inducing the "transverse" migration of the charged NPs which, at the end of the channel were sorted channel into a 96-well plate.

The electrophoretic mobility of spherical particles is given by $\mu_e = |z_i| e_0 / 6\pi\eta r_i$, where z_i is the valence of charged CdTe NPs , e_0 is the elementary charge, η is the dynamic viscosity of the medium, and r_i is the radius of the particles. Their mobility, therefore, depends on the particles' charge-to-size ratio and NPs with higher ratios move transversely more than those with smaller ratios. This difference in mobility enables separation of NPs by either size or surface charge.

Based on these principles, CdTe NPs were separated into relatively monodisperse fractions. Successful fractionation was evidenced by the fluorescence spectra of the particles (Fig. 9b). The original sample had a peak maximum at 615 nm (corresponding to 4.7 nm average NP diameter). The separated sample with red colored CdTe NPs fluoresced at 627 nm (which corresponds to 5.1 nm NPs), while the green colored fraction fluoresced at 564 nm (2.9 nm NPs). The red-fluorescing NPs were collected in the wells farthest from the main sample stream, indicating that these larger NPs have higher electrophoretic mobilities than smaller ones. The sizes of the purified samples were also directly measured using TEM.

The IEF gel electrophoresis technique was used by Arnaud et al. [89] to narrow the size distribution of 1.7 ± 0.8 nm water soluble gold NPs stabilized by mercaptosuccinic acid. NP solution was loaded directly onto an immobilized pH gradient (IPG) strip at pH 8. At this basic environment, the NPs were negatively charged and migrated to the anode until they reached a pH region corresponding to their effective pI. The voltage was ramped linearly from 0 to 1000 V within 2 h. Since the surface charge density and thus the repulsions between charged ligands increase with increasing particle size (decreasing curvature), the apparent pK_a of the ligands depends on particle size. Consequently, in the

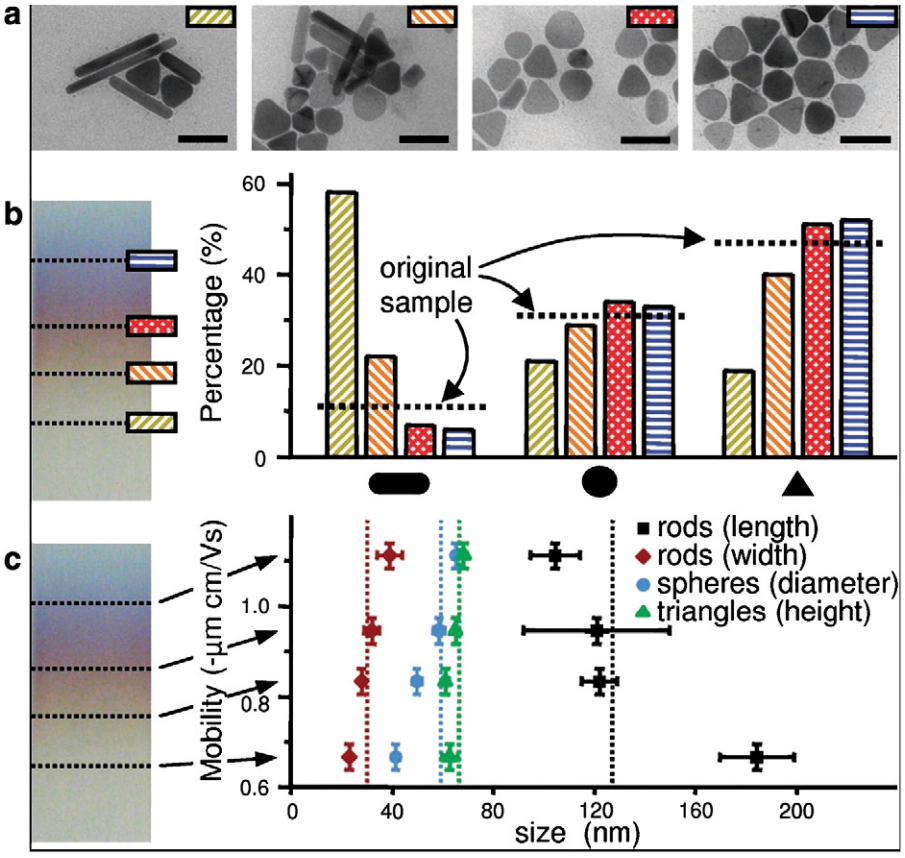

Fig. 8. (a) TEM images obtained from different parts of the gel lane containing silver nanoparticles (lane 1 in Fig. 10b). Scale bars correspond to 100 nm. (b) Statistics of the sample's composition in terms of rods, spheres, and triangles at four different locations. The first set of bars, for example, shows that silver rods are predominantly found in the slowest-moving fraction, where they account for 60% of the particles as compared to only 7% in the fastest-moving fraction. (c) Further analysis reveals separation of particles according to sphere diameter and rod aspect ratio. The average sphere diameter increases from 41 ± 2 nm in the slowest-moving fraction to 65 ± 2 nm in the fastest-moving fraction. The aspect ratio (length/width) of silver rods decreases from 8.3 ± 0.8 to 3.1 ± 0.7. For the triangles, no influence of size on the mobility was found. Vertical lines indicate the mean sizes in the original sample. Figure was taken from the Reference [87].

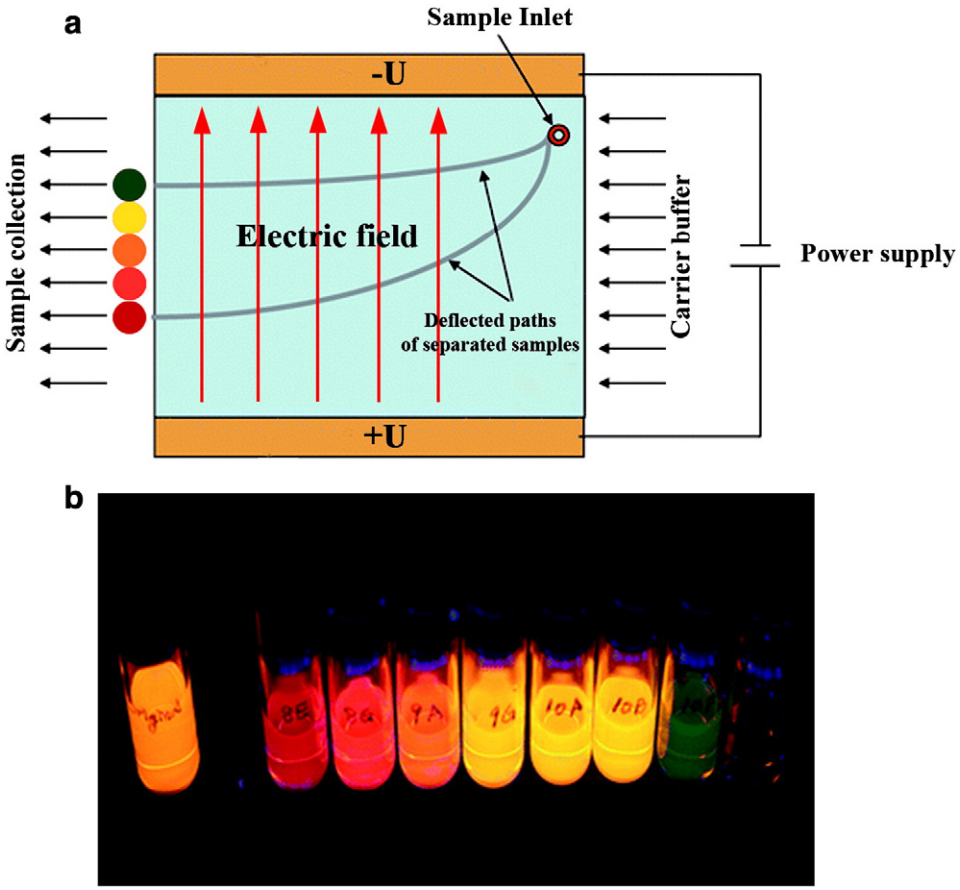

Fig. 9. (a). Schematic representation of a FFE setup. (b) Fluorescence of fractionated semiconductor CdTe nanoparticles under UV illumination. The leftmost vial contains the original mixture that appears orange under UV light. Figure was taken from the Reference [88].

region around pH = 5, the particles form distinct bands corresponding to the sizes of 1.7 ± 0.4 nm, 3.3 ± 0.4 nm and 4.9 ± 0.3 nm.

2.5. Selective precipitation

Size-selective precipitation, SSP, is a simple technique which allows for separating the NPs according to size-dependent physical and chemical properties, reactivity, and/or stability. Since these properties depend strongly on the surface chemistry of the NPs, SSP should be tailored to specific particle type/functionalization.

An illustrative example of SSP is the DNA-induced size-fractionation of gold nanoparticles developed by the Mirkin group. [90•] These authors discovered that the so-called melting temperature, T_m – that is, temperature above which the hybridized DNA duplexes in DNA-linked NP clusters disassemble ("melt") causing sharp transition from an aggregated to a dispersed phase – increases with NP size (Fig. 10a). This dependence was related to the number of possible connections between NPs. While DNA density on NP surface is constant and independent on NP size, the contact area between nanoparticles increases with particle size. As a result, large nanoparticles form more linkages with each other than small ones, and the temperature required to "melt"/separate them is higher.

These observations allowed for the separation of binary and ternary mixtures of differently sized (15, 30, 40, 50, 60 and 80 nm) NPs into separate batches with purity above 90% (Fig. 10b). Specifically, when the temperature was adjusted to above the T_m of smaller particles but below T_m of larger particles, only the latter ones aggregated. The sample was then centrifuged to precipitate the aggregates, which were then heated to dissociate into individual NP's. The smaller, unaggregated particles that remained in the original solution were isolated from the supernatant.

Oligonucleotides capping AuNPs were also used for NP separation by Zhao et al. [91] It was reported that oligonucleotide-capped AuNPs undergo reversible salt-induced aggregation, and that the concentration of salt at which aggregation commences depends on NP sizes — in particular, larger particles aggregate at lower salt concentration than the smaller particles. The salt-induced aggregation is due to the interplay between (i) van der Waals (vdW) attractions between NP cores (the magnitude of these interactions scales with particle size), and (ii) electrostatic repulsions between the negatively charged oligonucleotides. Importantly, unlike smaller charged ligands (e.g., citrates), large-nucleotides prevent close approach of the NPs' metal cores resulting in reversible aggregation such that upon dilution of the sample the particles redisperse. As an example, the authors performed several separations of bimodally distributed gold nanoparticles (10 and 40 nm, 20 and 40 nm, 10 and 20 nm). TEM analyses confirmed that the purity of smaller particles in the supernatant was above 99%, while that of larger particles in the precipitate, not smaller than 96%.

Although most popular in aqueous conditions, selective precipitation has also been proven to work well in organic solvents. Roberts et al. [92–94] developed a fractionation method allowing for a separation of nanoparticles by gas pressurization, using tunable solvent properties of CO_2-expanded hexane. As an illustration of this technique, a mixture of differently-sized CdSe/ZnS quantum dots was fractionated into differently colored fractions by changing the CO_2 pressure.[92] The changes of gas pressure affected the balance between NP solvation favoring particle dispersion [95] and attractive vdW forces driving particle aggregation. In a wider context, this method is a variant of antisolvent precipitation techniques [96,97] relying on fractional precipitation from a "good" solvent by addition of a "bad" one. Here, CO_2 miscible with hexane acts as a "bad" solvent diminishing the solvation of the particles in hexane and causing their precipitation due to vdW, size-dependent attractions.

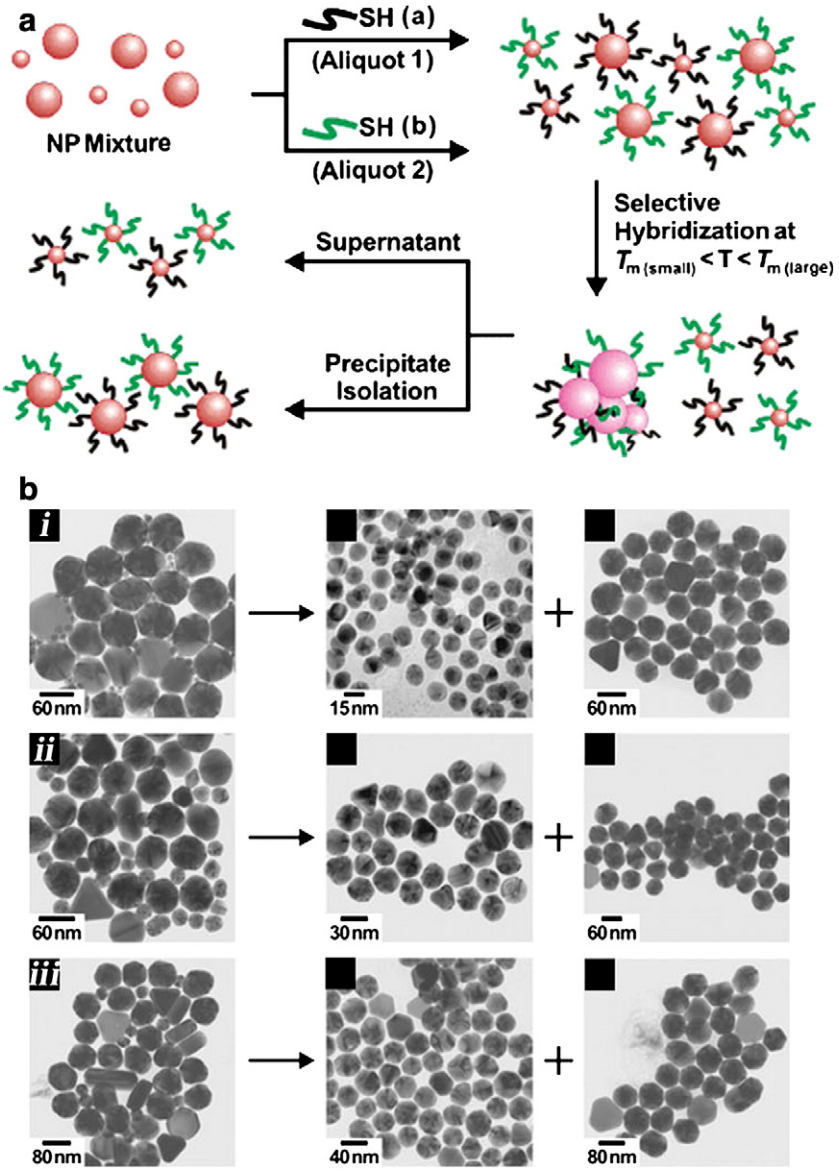

Fig. 10. (a) Schematic of the procedure for DNA-based size-selective precipitation of AuNPs. Two aliquots of a mixture containing small and large NPs (in 1:1 ratio) were modified with oligonucleotides (complementary to each other). The two samples were combined and allowed to selectively hybridize. Then, aggregates of large particles were separated from small NPs by centrifugation. (b) TEM images showing the samples before and after fractionation for mixtures containing different sizes of NPs: (i) 15 and 60 nm; (ii) 30 and 60 nm; (iii) 40 and 80 nm. Figure was taken from the Reference [90].

There are, however, several advantages of this gas-based method over traditional antisolvent precipitation. First, it is very easy to control the properties of a mixture by adjusting gas pressure. Second, CO_2-expanded liquids are easier to mix and precipitation occurs much faster than in the case of regular liquids (due to higher diffusivities and lower viscosities of the former). Therefore, additional centrifugation of NP aggregates can be omitted. From the economical point of view, gas pressurization uses less solvent and gas can be easily recycled by depressurization. Last but not least, multiple fractions of nanoparticles can be collected in a single experiment with no need of multiple mixing, separation and centrifugation steps necessary in liquid antisolvent precipitation techniques.

2.6. Membrane filtration

Filtration though a membrane is another alternative for the purification and size-fractionation of NPs. In this class of methods, retention and elution of an analyte depend on the size of membrane pores.

Akthakul et al. [98] fractionated AuNPs using a thin polymeric membrane made of graft copolymer with hydrophobic poly(vinylidene-fluoride) (PVDF) backbone and hydrophilic poly(oxyethylene methacrylate) (POEM) side chains. This membrane was characterized by bicontinous morphology and had uniformly sized PEO nanochannels surrounded by a PVDF matrix.

When a toluene solution containing polydisperse, octanethiol-modified AuNPs was filtered through the PEO/PVDF matrix, particles larger than 3.8 nm were retained on the membrane, while smaller ones passed through it freely. As a result, the size distribution improved from 3 ± 1 nm in the initial sample to 2.2 ± 0.7 nm in the filtrate. In an additional experiment, AuNPs were coated with a thicker octadecanethiol SAM such that the filtration cutoff decreased to 3.2 nm metal core diameter. Interestingly, the performance of the membrane could be changed by adjusting the polarity of the solvent swelling of PEO chains

and changing the diameter of the nanochannels. Using binary solvent mixtures, it was then possible to achieve a desired degree of swelling and NP diameter cutoff.

Sweeney et al. [99] have demonstrated that membrane filtration is also a good method for the size-fractionation of water soluble nanoparticles. They performed separate experiments in which they purified small AuNPs, separated binary mixtures into corresponding fractions, and finally fractionated polydisperse samples into several fractions characterized by different mean diameters of the metal cores. The scheme of the continuous filtration setup used in these experiments is depicted in Fig. 11. Briefly, a water-based NP sample was placed in a reservoir, from which it was drawn by a peristaltic pump into the filtration membrane. The rate of water addition to the reservoir was adjusted to match the rate of elution. Filtration was continued through multiple filtration volumes until reaching the desired rate of size separation or sample purity (one filtration volume is defined as the volume of material eluted equal to the hold-up volume in the reservoir).

In one example, a binary mixture of AuNPs (1.5 nm and 2.9 nm in 1:1 NP/NP ratio), was filtered with 10×15 mL of water through 50 kDa membrane (nominal molecular weight cutoff, MWCO, wherein a 50 kDa means the membrane will retain 90% of a globular protein with a molecular mass >50 kDa). The quality of separation was determined by TEM, which showed that retained fraction comprised 2.9 ± 1.0 nm NPs, while permeate had 1.5 ± 0.5 nm sized particles. The authors compared their filtration to other common techniques including dialysis extraction, centrifugation, and chromatography. They concluded that filtration yields nanoparticles of higher purity, in less time (~15 min vs. several days) and with less waste (4 L of H_2O/g of product vs. 15 L of solvent/g of product) than any of these other methods.

Finally, the same authors have shown that a sample containing polydisperse NPs could be fractionated with sequential filtrations through membranes characterized by different MWCO values. In their work, the initial solution was first filtered through a 70 kDa membrane which retained the largest, 2.9 ± 0.9 nm, particles. The remaining permeate was then filtered through a 50 kDa membrane (with smaller pores), and the retained particles were again collected; these particles had a size distribution 2.6 ± 0.9 nm. The operation was repeated with 30 kDa and 10 kDa membranes retaining progressively smaller and smaller NPs (2.5 ± 0.9 nm and 2.0 ± 0.7 nm, respectively).

In general, the greatest advantages of membrane filtrations are minimal equipment requirements and potential scalability. On the other hand, it should be remembered that these methods are only as good as the quality of the porous membrane: the better the pore uniformity, the better the quality of NP separation.

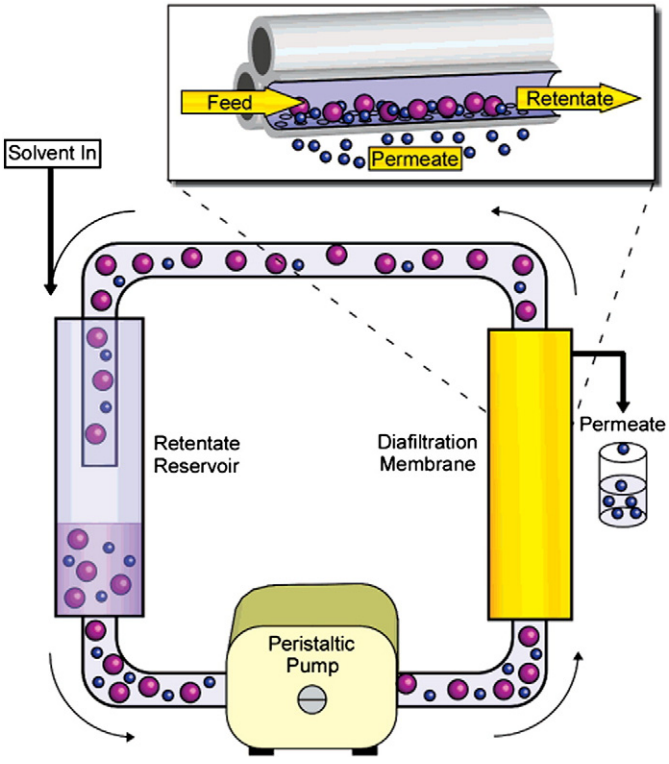

Fig. 11. Scheme of a continuous filtration setup. Sample and makeup solution are introduced into the retentate reservoir. The solution is pumped by a peristaltic pump through the filtration membrane. Small-molecule impurities or small nanoparticles (blue) are eluted in the permeate, while the large NPs (purple) are retained. The expanded view illustrates a hollow-fiber-type filtration membrane eluting small impurities while retaining larger NPs. Figure was taken from the Reference [99].

2.7. Extraction

Extraction is a method to separate compounds based on their relative solubilities in two different, immiscible liquid phases, usually water and an organic solvent. This method has been used widely for separation and purification of organic and inorganic compounds. Recently, Wilson et al. [100] reported selective extraction of Au and Ag dendrimer-encapsulated NPs (DENs). In this work, sixth-generation, hydroxyl-terminated PAMAM dendrimers (G6-OH) covering either 147-atom Au NPs (G6-OH(Au_{147})) [101] or 110 atom Ag NPs (G6-OH(Ag_{110})) [102] were synthesized. High resolution transmission electron microscopy (HRTEM) indicated that the resulting DENs had average diameters of 1.4 ± 0.4 nm for (G6-OH(Au_{147}) and 1.7 ± 0.4 nm for (G6-OH(Ag_{110})). The mixture of these DENs had a size distribution 1.6 ± 0.3 nm and composition 57% G6-OH(Au147)/43% G6-OH(Ag110) (determined by energy-dispersive X-ray spectroscopy, EDS). Selective extraction of Ag DENs was achieved by adding *n*-decanoic acid/hexane solution to an aqueous mixture of G6-OH(Ag_{110}) and G6-OH (Au_{147}) DENs. After stirring for 30 s, the originally colorless organic phase turned yellow, which is characteristic of small silver NPs. Indeed, the extracted fraction contained 95 ± 6% Ag and 5 ± 6% Au DENs, and its size distribution matched that of pure Ag DENs. After removing the organic phase, ascorbic acid was added to the aqueous phase (to increased the ionic strength) followed by the extraction of G6-OH(Au_{147}) with *n*-dodecanethiol/hexane solution. The fraction obtained after this second extraction had a composition 8 ± 6% Ag and 92 ± 6% Au and size distribution matching that of pure Au DENs. The authors proposed that in this method, a selective separation was possible owing to the fact that *n*-alkanoic acids (here, *n*-decanoic acid) have higher affinity for chemisorption onto Ag than onto Au surface.

Another extraction method for reversible separation/concentration and dispersion of various NPs based on cloud point extraction (CPE) was proposed by Liu et al. [103]. It is well known that surface-active chemicals can assemble into colloidal-sized clusters called micelles. During their formation, these micelles can encapsulate various substances thus segregating them from the bulk solution. The solubility of non-ionic or zwitterionic surfactants in water phase is dramatically depressed above a well-defined temperature called cloud point temperature, CPT. Above CPT, a solution separates into a concentrated phase containing most of the surfactant (the surfactant-rich phase) and a dilute aqueous phase. CPE is based on the affinity of compounds/particles of interest toward the surfactant — this affinity then determines the extent of partitioning between the surfactant-rich and the surfactant-poor phases.

In their work, Liu and co-workers extracted/concentrated several types of NPs (capping reagents listed in parentheses): Au NPs (trisodium citrate), Ag NPs (polyvinylpyrrolidone), C_{60} fullerene, TiO_2, Fe_3O_4 NPs (humic acid), CdSe/ZnS (polyethylene glycol), and SWCNTs (dispersed with sodium dodecylbenzene sulfonate). Triton X-114 sufactant (3.6 mM) and NaCl (3.4 mM) were added to the NP solution, which was then heated above the CPT (23–25 °C). Owing to the NP-micelle interactions, nanoparticles were extracted from the aqueous suspension (10 mL) into the surfactant rich phase (0.1 mL). The samples

were centrifuged, and the concentrated NPs were redispersed into the aqueous phase by cooling to a temperature below CPT. The authors verified that at least ten consecutive separation/dispersion cycles were possible and that the NPs could be stored in the Triton X-114 rich phase for over 2 months without any evidence of aggregation or morphology/size change.

2.8. Miscellaneous

In addition to popular methods described in previous sections, many authors have proposed less "conventional" yet effective separation strategies. Since limited space prevents us from a detailed discussion of all these methods, we have chosen those which we believe are most ingenious or effective.

Williams et al. [104] used supercritical ethane in size-selective separation of alkanethiol-stabilized gold nanoparticles. In contrast to selective precipitation techniques, this method relies on fractional, size-dependent redispersion of NPs in supercritical ethane. Specifically, nanoparticles with sizes ranging from 1 to 5 nm were fractionated at 318 K under adjustable pressures ranging from 50 to 276 bar. A vial containing solid NPs was placed into a stainless steel vessel, which was then pressurized with ethane and heated above ethane's critical point. Pressure was maintained for 18 h in order to completely disperse the particles — importantly, the sizes of the dispersed NPs depended on the pressure applied (since the properties of the supercritical fluid depend on pressure). After collection of a NP fraction, the pressurized fluid was slowly released through and precipitated into a layer of acetone, and the NPs were collected by filtration. When the procedure was repeated under a different pressure of ethane, differently sized NPs were retrieved.

Jana developed a simple and efficient method in which monodisperse nanorods are separated from a mixture of differently sized rods, spheres and plates by surfactant assisted ordering.[105] Addition of a surfactant (cetyltrimethylammonium bromide, CTAB) to a concentrated mixture caused precipitation of rods and platelets from the mixture, leaving the spheres in solution. Importantly, longer rods precipitated before shorter ones, followed by platelets. This phenomenon was attributed to the formation of liquid-crystal-like nanorod aggregates which, due to their size and mass, precipitated from solution.

An interesting approach involving depletion forces was very recently demonstrated by Park et al. [106] and also by Hollamby et al.[107] These authors reported shape and size separation of Au NPs and attributed the phenomenon to micelle-induced depletion interactions between particles. The entropic, short-ranged depletion attractions between the NPs originated from the presence of micelles in solution. Remarkably, NPs of different sizes could be induced to aggregate by adjusting micelle concentration. When surfactant concentration was optimized and the NP flocculates were separated by centrifugation or gravitational sedimentation, the NPs of the same mass but different shapes were purified. Using this technique, it was possible to separate spherical particles, as well as long and short rods from their mixture.

Khanal and Zubarev [108] capitalized on shape-dependent reactivity of nanoparticulated species in order to purify a binary solution of nanorods and platelets. Specifically, when Au(III)/CTAB complex was added to the mixture, the platelets were transformed into smaller nanodisks. While these disks were readily soluble and stable in solution, the larger nanorods gradually precipitated and were isolated with purity above 99%. The nanodisks left behind were 90% pure and could be converted back into platelets by treatment with a growth solution containing Au(I) ions and ascorbic acid. The outcome of experiment was monitored by TEM, UV–Vis, and NIR spectroscopy.

Kang et al. [109] developed an ultrasound-assisted phase transfer method for the separation of nanoparticles of different shapes from byproducts in post-reaction mixtures. The method was based on a two-phase liquid system composed of a polar phase (alcohol C1–C3/water,) and a nonpolar phase (alkane C5–C10/ethanol). The separation phenomenon was due to the combination of the interfacial surface tension and the dynamic equilibrium established between nanomaterials of different weights. Under sonication conditions, transfer from alcohol/water to alcohol/alkane phase took place. By using this procedure the authors have shown successful separation of various silicon nanostructures: wires, spheres, ribbons, and cones. When the system was sonicated, these nanostructures could be separated either from different layers or from the liquid/liquid interface.

Finally, our own group used the so-called periodic precipitation, PP, phenomenon to separate particles of different sizes and dispersities.[110] In classical periodic-precipitation, inorganic salts diffusing in opposite directions through a gel matrix form distinct zones/bands of precipitation (these bands are often called Liesegang rings). We have shown that a similar phenomenon is observed when the gel supports diffusion of oppositely charged nanoparticles (Fig. 12a), which precipitate when their charges are compensated [40,111,112] (Fig. 12b). In contrast to the salt-based PP systems where all participating ions/molecules of the given type have identical sizes, the NPs are inherently polydisperse. An interesting consequence of NP polydispersity is illustrated in Fig. 12 c,d, where NPs of one type are significantly more polydisperse than the other (but both have the same average diameters). For example, when more polydisperse NPs are delivered into a gel containing less polydisperse NPs (Fig. 12c), the first ring collects the largest particles from the outer electrolyte. In the

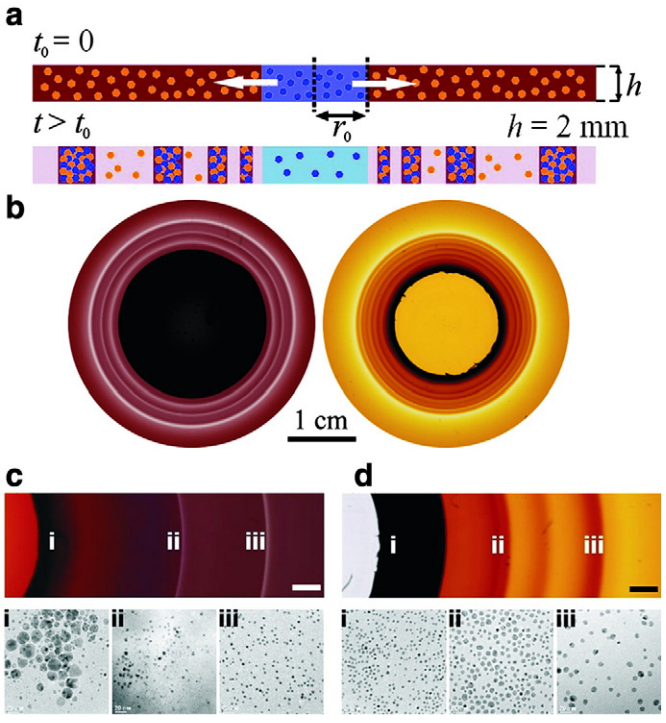

Fig. 12. (a) Cross-sectional view and typical dimensions of the gel layer supporting periodic precipitation of oppositely charged nanoparticles (colored blue and orange). Negative charges are introduced by covering the NPs with a monolayer of 11-mercaptoundecanoic acid (MUA); positive charges with N,N,N-trimethyl(11-mercaptoundecyl)ammonium chloride (TMA). (b) Examples of ring structures formed by (left image) 7.5 nm AuTMA (10.43 mM) NPs delivered to a gel containing 7.4 nm AuMUAs (2.26 mM) and (right image) 9.7 nm AgTMA (9.47 mM) particles delivered into a gel soaked with 7.4 nm AgMUAs (2.08 mM). The characteristic hues of the patterns derive from the surface plasmon resonance (SPR) of the particles (red-violet for AuNPs and yellow-orange for AgNPs). (c,d) Optical micrographs of the ring patterns and TEM's of particles extracted from different rings. (c) AgTMA (7.41 mM, 9.7 nm in diameter with polydispersity $\sigma = 40\%$) delivered into a gel containing AuMUA NPs (1.79 mM, 8.0 nm, $\sigma = 18\%$). Polydispersity of the NPs is 38.2% in the first ring and decreases to 16.8% in the third ring. (d) AuTMA (9.47 mM, 7.4 nm, $\sigma = 6\%$) delivered into a gel containing AgMUA (2.08 mM, 7.4 nm, $\sigma = 42\%$). NP polydispersity is 11.7% in the first ring and increases to 43.0% in the third ring. Figure was taken from the Reference [110].

opposite case (i.e., monodisperse NPs delivered into a gel containing polydisperse NPs; Fig. 12d, the first ring is the least polydisperse and contains smaller particles. As we have shown, these trends can be explained within the framework of reaction-diffusion models [110,113,114] by an interplay between particle diffusion (smaller for larger particles) and electrostatic particle–particle interactions.

3. Conclusions

Size and shape uniformity of nanoparticulate objects is important in several branches of nanotechnology. Since vast majority of wet "nanosynthetic" procedures yield polydisperse particles, there is a need for effective purification/separation techniques that would be widely applicable, high-throughput, and inexpensive. While no single method we have described meets all of these criteria, the repertoire of nanoseparation techniques is quite diverse and ranges from those adapted from traditional separations science (chromatography, extraction, filtration), to methods based on nanosclae specific phenomena (differential reactivity of differently shaped NPs, chemical self-organization). The current review is an attempt to catalog and categorize these approaches. Still, it does not provide ready-to-apply prescriptions on how to separate any desired mixture of nanocomponents. Developing such *a priori* prescriptions appears to be the main challenge for the future research on nanoseparations.

Acknowledgements

This work was supported by the Non-equilibrium Energy Research Center (NERC) which is an Energy Frontier Research Center funded by the U.S. Department of Energy, Office of Science, Office of Basic Energy Sciences under Award Number DE-SC0000989.

References

[1] Sun YG, Xia YN. Shape-controlled synthesis of gold and silver nanoparticles. Science 2002;298:2176–9.* This paper reports the large scale chemical synthesis of uniform and monodisperse silver and gold nanocubes and truncated nanocubes.
[2] Manna L, Scher EC, Alivisatos AP. Synthesis of soluble and processable rod-, arrow-, teardrop-, and tetrapod-shaped CdSe nanocrystals. J Am Chem Soc 2000;122:12700–6.
[3] Walker DA, Browne KP, Kowalczyk B, Grzybowski BA. Self-assembly of nanotriangle super lattices facilitated by repulsive electrostatic interactions. Angew Chem Int Ed 2010;49:6760–3.
[4] Klajn R, Pinchuk AO, Schatz GC, Grzybowski BA. Synthesis of heterodimeric sphere-prism nanostructures via metastable gold supraspheres. Angew Chem Int Ed 2007;46:8363–7.
[5] Teranishi T, Miyake M. Size control of palladium nanoparticles and their crystal structures. Chem Mater 1998;10:594–600.
[6] Pileni MP. The role of soft colloidal templates in controlling the size and shape of inorganic nanocrystals. Nat Mater 2003;2:145–50.** Paper (progress report) discussing the state-of-the-art surfactant-assisted methods for the size controlled syntheses of NPs.
[7] Sun SH, Zeng H. Size-controlled synthesis of magnetite nanoparticles. J Am Chem Soc 2002;124:8204–5.
[8] Tao F, Grass ME, Zhang YW, et al. Evolution of structure and chemistry of bimetallic nanoparticle catalysts under reaction conditions. J Am Chem Soc 2010;132:8697–703.
[9] Yan JM, Zhang XB, Akita T, et al. One-step seeding growth of magnetically recyclable Au@Co core-shell nanoparticles: highly efficient catalyst for hydrolytic dehydrogenation of ammonia borane. J Am Chem Soc 2010;132:5326–7.
[10] Mazumder V, Chi MF, More KL, Sun SH. Core/shell Pd/FePt nanoparticles as an active and durable catalyst for the oxygen reduction reaction. J Am Chem Soc 2010;132:7848–9.
[11] Kang YJ, Murray CB. Synthesis and electrocatalytic properties of cubic Mn – Pt nanocrystals (nanocubes). J Am Chem Soc 2010;132:7568–9.
[12] Mallin MP, Murphy CJ. Solution-phase synthesis of sub-10 nm Au–Ag alloy nanoparticles. Nano Lett 2002;2:1235–7.
[13] Ruckenstein E, Li ZF. Surface modification and functionalization through the self-assembled monolayer and graft polymerization. Adv Colloid Interface Sci 2005;113:43–63.
[14] Gref R, Couvreur P, Barratt G, Mysiakine E. Surface-engineered nanoparticles for multiple ligand coupling. Biomaterials 2003;24:4529–37.
[15] Dubois F, Mahler B, Dubertret B, et al. A versatile strategy for quantum dot ligand exchange. J Am Chem Soc 2007;129:482–3.
[16] Lin CAJ, Sperling RA, Li JK, et al. Design of an amphiphilic polymer for nanoparticle coating and functionalization. Small 2008;4:334–41.
[17] Klajn R, Stoddart JF, Grzybowski BA. Nanoparticles functionalised with reversible molecular and supramolecular switches. Chem Soc Rev 2010;39:2203–37.** Thorough review article on nanoparticles functionalized with SAMs of molecular and supramolecular switches for reversible and dynamic NP self-assembly.
[18] Jiang W, Kim BYS, Rutka JT, Chan WCW. Nanoparticle-mediated cellular response is size-dependent. Nat Nanotechnol 2008;3:145–50.
[19] Park TJ, Papaefthymiou GC, Viescas AJ, et al. Size-dependent magnetic properties of single-crystalline multiferroic $BiFeO_3$ nanoparticles. Nano Lett 2007;7:766–72.
[20] Kennedy MK, Kruis FE, Fissan H, et al. Tailored nanoparticle films from monosized tin oxide nanocrystals: particle synthesis, film formation, and size-dependent gas-sensing properties. J Appl Phys 2003;93:551–60.
[21] Nanda J, Narayan KS, Kuruvilla BA, et al. Sizable photocurrent and emission from solid state devices based on CdS nanoparticles. Appl Phys Lett 1998;72:1335–7.
[22] Park SW, Jang JT, Cheon J, et al. Shape-dependent compressibility of TiO_2 anatase nanoparticles. J Phys Chem C 2008;112:9627–31.
[23] Zheng C, Du YH, Feng M, Zhan HB. Shape dependence of nonlinear optical behaviors of nanostructured silver and their silica gel glass composites. Appl Phys Lett 2008;93:143108.
[24] Anker JN, Hall WP, Lyandres O, et al. Biosensing with plasmonic nanosensors. Nat Mater 2008;7:442–53.** Review article disscussing the applications of plasmonic metal NPs as biosensors.
[25] Klajn R, Browne KP, Soh S, Grzybowski BA. Nanoparticles That "Remember" Temperature. Small 2010;6:1385–7.
[26] Roy I, Ohulchanskyy TY, Pudavar HE, et al. Ceramic-based nanoparticles entrapping water-insoluble photosensitizing anticancer drugs: a novel drug-carrier system for photodynamic therapy. J Am Chem Soc 2003;125:7860–5.
[27] Peer D, Karp JM, Hong S, et al. Nanocarriers as an emerging platform for cancer therapy. Nat Nanotechnol 2007;2:751–60.** Review article focusing on rational design of nanoscopic carriers and molecules for clinical application in targeting tumours.
[28] Nakanishi H, Grzybowski BA. Supercapacitors based on metal electrodes prepared from nanoparticle mixtures at room temperature. J Phys Chem Lett 2010;1:1428–31.
[29] Bliznyuk V, Ruhstaller B, Brock PJ, et al. Self-assembled nanocomposite polymer light-emitting diodes with improved efficiency and luminance. Adv Mater 1999;11:1257–61.
[30] Park JH, Lim YT, Park OO, et al. Polymer/Gold nanoparticle nanocomposite light-emitting diodes: enhancement of electroluminescence stability and quantum efficiency of blue-light-emitting polymers. Chem Mater 2004;16:688–92.
[31] Barnes WL, Dereux A, Ebbesen TW. Surface plasmon subwavelength optics. Nature 2003;424:824–30.
[32] Hasobe T, Imahori H, Kamat PV, et al. Photovoltaic cells using composite nanoclusters of porphyrins and fullerenes with gold nanoparticles. J Am Chem Soc 2005;127:1216–28.
[33] Sun BQ, Marx E, Greenham NC. Photovoltaic devices using blends of branched CdSe nanoparticles and conjugated polymers. Nano Lett 2003;3:961–3.
[34] Tseng RJ, Tsai CL, Ma LP, Ouyang JY. Digital memory device based on tobacco mosaic virus conjugated with nanoparticles. Nat Nanotechnol 2006;1:72–7.
[35] Chon JWM, Bullen C, Zijlstra P, Gu M. Spectral encoding on gold nanorods doped in a silica sol–gel matrix and its application to high-density optical data storage. Adv Funct Mater 2007;17:875–80.
[36] Maneeprakorn W, Malik MA, O'Brien P. Developing chemical strategies for the assembly of nanoparticles into mesoscopic objects. J Am Chem Soc 2010;132:1780–1.
[37] Wei YH, Bishop KJM, Kim J, et al. Making use of bond strength and steric hindrance in nanoscale "synthesis". Angew Chem Int Ed 2009;48:9477–80.
[38] Wei YH, Klajn R, Pinchuk AO, Grzybowski BA. Synthesis, shape control, and optical properties of hybrid Au/Fe_3O_4 "nanoflowers". Small 2008;4:1635–9.
[39] Wang H, Brandl DW, Nordlander P, Halas NJ. Plasmonic nanostructures: artificial molecules. Acc Chem Res 2007;40:53–62.
[40] Kalsin AM, Kowalczyk B, Smoukov SK, et al. Ionic-like behavior of oppositely charged nanoparticles. J Am Chem Soc 2006;128:15046–7.
[41] Kalsin AM, Kowalczyk B, Wesson P, et al. Studying the thermodynamics of surface reactions on nanoparticles by electrostatic titrations. J Am Chem Soc 2007;129:6664–5.
[42] Kalsin AM, Pinchuk AO, Smoukov SK, et al. Electrostatic aggregation and formation of core-shell suprastructures in binary mixtures of charged metal nanoparticles. Nano Lett 2006;6:1896–903.
[43] Pinchuk AO, Kalsin AM, Kowalczyk B, et al. Modeling of electrodynamic interactions between metal nanoparticles aggregated by electrostatic interactions into closely-packed clusters. J Phys Chem C 2007;111:11816–22.
[44] Vestal CR, Zhang ZJ. Synthesis of CoCrFeO4 nanoparticles using microemulsion methods and size-dependent studies of their magnetic properties. Chem Mater 2002;14:3817–22.
[45] Berquo TS, Banerjee SK, Ford RG, et al. High crystallinity Si-ferrihydrite: an insight into its Neel temperature and size dependence of magnetic properties. J Geophys Res Solid Earth 2007;112.
[46] Narayanan R, El-Sayed MA. Shape-dependent catalytic activity of platinum nanoparticles in colloidal solution. Nano Lett 2004;4:1343–8.
[47] Wei YH, Han SB, Kim J, et al. Photoswitchable catalysis mediated by dynamic aggregation of nanoparticles. J Am Chem Soc 2010;132:11018–20.
[48] Pan Y, Neuss S, Leifert A, et al. Size-dependent cytotoxicity of gold nanoparticles. Small 2007;3:1941–9.

[49] Euliss LE, DuPont JA, Gratton S, DeSimone J. Imparting size, shape, and composition control of materials for nanomedicine. Chem Soc Rev 2006;35:1095–104.
[50] Wang W, Asher SA. Photochemical incorporation of silver quantum dots in monodisperse silica colloids for photonic crystal applications. J Am Chem Soc 2001;123:12528–35.
[51] Nakanishi H, Bishop KJM, Kowalczyk B, et al. Photoconductance and inverse photoconductance in films of functionalized metal nanoparticles. Nature 2009;460:371–5.** This paper reports the first experimentally observed evidence of negative photocondutance effect in films of plasmonic nanoparticles.
[52] Wang ZX, Tan BE, Hussain I, et al. Design of polymeric stabilizers for size-controlled synthesis of monodisperse gold nanoparticles in water. Langmuir 2007;23:885–95.
[53] Hussain I, Graham S, Wang ZX, et al. Size-controlled synthesis of near-monodisperse gold nanoparticles in the 1–4 nm range using polymeric stabilizers. J Am Chem Soc 2005;127:16398–9.
[54] Taleb A, Petit C, Pileni MP. Synthesis of highly monodisperse silver nanoparticles from AOT reverse micelles: a way to 2D and 3D self-organization. Chem Mater 1997;9:950–9.
[55] Murray CB, Norris DJ, Bawendi MG. Synthesis and characterization of nearly monodisperse CdE (E = S, Se, Te) semiconductor nanocrystallites. J Am Chem Soc 1993;115:8706–15.
[56] Adair JH, Suvaci E. Morphological control of particles. Curr Opin Colloid Interface Sci 2000;5:160–7.** Review article on theoretical and practical aspects of synthesis of anisotropic nanoparticles with shape and size control.
[57] Kumar S, Nann T. Shape control of II-VI semiconductor nanomateriats. Small 2006;2:316–29.* Review article on the most popular methods for the synthesis and shape evolution of quantum dots.
[58] Murphy CJ, San TK, Gole AM, et al. Anisotropic metal nanoparticles: synthesis, assembly, and optical applications. J Phys Chem B 2005;109:13857–70.
[59] Fletcher D. Fine particle high-gradient magnetic entrapment. IEEE Trans Magn 1991;27:3655–77.
[60] Bishop KJM, Wilmer CE, Soh S, Grzybowski BA. Nanoscale forces and their uses in self-assembly. Small 2009;5:1600–30.** Comprehensive and systematic review of the forces acting between nanosized objects in which theoretical considerations are illustrated with most pertinent experiments.
[61] Moeser GD, Roach KA, Green WH, et al. High-gradient magnetic separation of coated magnetic nanoparticles. AlChE J 2004;50:2835–48.
[62] Ditsch A, Lindenmann S, Laibinis PE, et al. High-gradient magnetic separation of magnetic nanoclusters. Ind Eng Chem Res 2005;44:6824–36.
[63] Yavuz CT, Mayo JT, Yu WW, et al. Low-field magnetic separation of monodisperse Fe_3O_4 nanocrystals. Science 2006;314:964–7.* The article describes the method for size separation of magnetic NPs in a low-field and the application of this method to water waste treatment.
[64] Latham AH, Freitas RS, Schiffer P, Williams ME. Capillary magnetic field flow fractionation and analysis of magnetic nanoparticles. Anal Chem 2005;77:5055–62.
[65] Rheinlander T, Kotitz R, Weitschies W, Semmler W. Different methods for the fractionation of magnetic fluids. Colloid Polym Sci 2000;278:259–63.
[66] Jimenez VL, Leopold MC, Mazzitelli C, et al. HPLC of monolayer-protected gold nanoclusters. Anal Chem 2003;75:199–206.
[67] Wilcoxon JP, Martin JE, Provencio P. Size distributions of gold nanoclusters studied by liquid chromatography. Langmuir 2000;16:9912–20.
[68] Siebrands T, Giersig M, Mulvaney P, Fischer CH. Steric exclusion chromatography of nanometer-sized gold particles. Langmuir 1993;9:2297–300.
[69] Kirkland JJ. High-performance size-exclusion liquid-chromatography of inorganic colloids. J Chromatogr 1979;185:273–88.
[70] Fischer CH, Lilie J, Weller H, et al. Photochemistry of colloidal semiconductors.29. Fractionation of Cds sols of small particles by exclusion chromatography. Berichte Der Bunsen-Gesellschaft-Physical Chemistry. Chem Phys 1989;93:61–4.
[71] Wei GT, Liu FK. Separation of nanometer gold particles by size exclusion chromatography. J Chromatogr A 1999;836:253–60.
[72] Liu FK, Wei GT. Effect of mobile-phase additives on separation of gold nanoparticles by size-exclusion chromatography. Chromatographia 2004;59:115–9.
[73] Wei GT, Liu FK, Wang CRC. Shape separation of nanometer gold particles by size-exclusion chromotography. Anal Chem 1999;71:2085–91.
[74] Al-Somali AM, Krueger KM, Falkner JC, Colvin VL. Recycling size exclusion chromatography for the analysis and separation of nanocrystalline gold. Anal Chem 2004;76:5903–10.
[75] Krueger KM, Al-Somali AM, Falkner JC, Colvin VL. Characterization of nanocrystalline CdSe by size exclusion chromatography. Anal Chem 2005;77:3511–5.
[76] Novak JP, Nickerson C, Franzen S, Feldheim DL. Purification of molecularly bridged metal nanoparticle arrays by centrifugation and size exclusion chromatography. Anal Chem 2001;73:5758–61.
[77] Brakke, M.K. Density Gradient Centrifugation And its Application to Plant Viruses. In: Advances in Virus Research, 1960, pp. 193-224.
[78] Arnold MS, Stupp SI, Hersam MC. Enrichment of single-walled carbon nanotubes by diameter in density gradients. Nano Lett 2005;5:713–8.* Paper describing application of density gradient ultracentrifugation in separation of single-walled carbon nanotubes with diameter size distributions as narrow as 0.02 nm.
[79] Arnold MS, Green AA, Hulvat JF, et al. Sorting carbon nanotubes by electronic structure using density differentiation. Nat Nanotechnol 2006;1:60–5.
[80] Sorensen SB, Pedersen TG, Ottesen M. Fractionation of protein-components from beer by density gradient centrifugation. Carlsberg Res Commun 1982;47:227–31.
[81] Sun X, Zaric S, Daranciang D, et al. Optical properties of ultrashort semiconducting single-walled carbon nanotube capsules down to sub-10 nm. J Am Chem Soc 2008;130:6551–5.
[82] Sun XM, Tabakman SM, Seo WS, et al. Separation of nanoparticles in a density gradient: FeCo@C and gold nanocrystals. Angew Chem Int Ed 2009;48:939–42.
[83] Chen G, Wang Y, Tan LH, et al. High-purity separation of gold nanoparticle dimers and trimers. J Am Chem Soc 2009;131:4218–9.
[84] Sharma V, Park K, Srinivasarao M. Shape separation of gold nanorods using centrifugation. Proc Natl Acad Sci USA 2009;106:4981–5.
[85] Westermeier R. Electrophoresis in practice. Wiley-VCH; 2005.
[86] Wagner H. Free-flow electrophoresis. Nature 1989;341:669–70.
[87] Hanauer M, Pierrat S, Zins I, et al. Separation of nanoparticles by gel electrophoresis according to size-and shape. Nano Lett 2007;7:2881–5.
[88] Ho SS, Critchley K, Lilly GD, et al. Free flow electrophoresis for the separation of CdTe nanoparticles. J Mater Chem 2009;19:1390–4.
[89] Arnaud I, Abid JP, Roussel C, Girault HH. Size-selective separation of gold nanoparticles using isoelectric focusing electrophoresis (IEF). Chem Commun 2005:787–8.
[90] Lee JS, Stoeva SI, Mirkin CA. DNA-induced size-selective separation of mixtures of gold nanoparticles. J Am Chem Soc 2006;128:8899–903.* Paper disscusses a size-separation technique of binary and ternary mixtures of gold nanoparticles based on size-selevtive aggregation of DNA-functionalized NPs.
[91] Zhao WY, Lin L, Hsing IM. Nucleotide-mediated size fractionation of gold nanoparticles in aqueous solutions. Langmuir 2010;26:7405–9.
[92] Anand M, Odom LA, Roberts CB. Finely controlled size-selective precipitation and separation of CdSe/ZnS semiconductor nanocrystals using CO_2-Gas-Expanded liquids. Langmuir 2007;23:7338–43.
[93] McLeod MC, Anand M, Kitchens CL, Roberts CB. Precise and rapid size selection and targeted deposition of nanoparticle populations using CO_2 gas expanded liquids. Nano Lett 2005;5:461–5.
[94] Saunders SR, Roberts CB. Size-selective fractionation of nanoparticles at an application scale using CO_2 gas-expanded liquids. Nanotechnology 2009;20:475605.
[95] Anand M, McLeod MC, Bell PW, Roberts CB. Tunable solvation effects on the size-selective fractionation of metal nanoparticles in CO_2 gas-expanded solvents. J Phys Chem B 2005;109:22852–9.
[96] Vossmeyer T, Katsikas L, Giersig M, et al. Cds nanoclusters — synthesis, characterization, size-dependent oscillator strength, temperature shift of the excitonic-transition energy, and reversible absorbency shift. J Phys Chem 1994;98:7665–73.
[97] Rogach AL, Kornowski A, Gao MY, et al. Synthesis and characterization of a size series of extremely small thiol-stabilized CdSe nanocrystals. J Phys Chem B 1999;103:3065–9.
[98] Akthakul A, Hochbaum AI, Stellacci F, Mayes AM. Size fractionation of metal nanoparticles by membrane filtration. Adv Mater 2005;17:532–5.
[99] Sweeney SF, Woehrle GH, Hutchison JE. Rapid purification and size separation of gold nanoparticles via diafiltration. J Am Chem Soc 2006;128:3190–7.
[100] Wilson OM, Scott RWJ, Garcia-Martinez JC, Crooks RM. Separation of dendrimer-encapsulated Au and Ag nanoparticles by selective extraction. Chem Mater 2004;16:4202–4.
[101] Kim YG, Oh SK, Crooks RM. Preparation and characterization of 1–2 nm dendrimer-encapsulated gold nanoparticles having very narrow size distributions. Chem Mater 2004;16:167–72.
[102] Zhao MQ, Crooks RM. Intradendrimer exchange of metal nanoparticles. Chem Mater 1999;11:3379–85.
[103] Liu JF, Liu R, Yin YG, Jiang GB. Triton X-114 based cloud point extraction: a thermoreversible approach for separation/concentration and dispersion of nanomaterials in the aqueous phase. Chem Commun 2009:1514–6.
[104] Williams DP, Satherley J. Size-selective separation of polydisperse gold nanoparticles in supercritical ethane. Langmuir 2009;25:3743–7.
[105] Jana NR. Nanorod shape separation using surfactant assisted self-assembly. Chem Commun 2003:1950–1.
[106] Park K, Koerner H, Vaia RA. Depletion-induced shape and size selection of gold nanoparticles. Nano Lett 2010;10:1433–9.
[107] Hollamby MJ, Eastoe J, Chemelli A, et al. Separation and purification of nanoparticles in a single step. Langmuir 2010;26:6989–94.
[108] Khanal BP, Zubarev ER. Purification of high aspect ratio gold nanorods: complete removal of platelets. J Am Chem Soc 2008;130:12634–5.
[109] Kang ZH, Tsang CHA, Ma DDD, et al. Nanomaterials separation by an ultrasonic-assisted phase transfer method. Chem Phys Lett 2008;455:252–5.
[110] Lagzi I, Kowalczyk B, Grzybowski BA. Liesegang rings engineered from charged nanoparticles. J Am Chem Soc 2010;132:58–60.
[111] Kalsin AM, Fialkowski M, Paszewski M, et al. Electrostatic self-assembly of binary nanoparticle crystals with a diamond-like lattice. Science 2006;312:420–4.
[112] Bishop KJM, Grzybowski BA. "Nanoions": fundamental properties and analytical applications of charged nanoparticles. Chemphyschem 2007;8:2171–6.
[113] Soh S, Byrska M, Kandere-Grzybowska K, Grzybowski BA. Reaction–diffusion systems in intracellular molecular transport and control. Angew Chem Int Ed 2010;49:4170–98.
[114] Grzybowski BA, Bishop KJM, Campbell CJ, et al. Micro- and nanotechnology via reaction–diffusion. Soft Matter 2005;1:114–28.